nature climate change

Article

https://doi.org/10.1038/s41558-023-01884-1

Fast upper-level jet stream winds get faster under climate change

Received: 20 April 2023

Accepted: 31 October 2023

Published online: 30 November 2023

Check for updates

Tiffany A. Shaw [1] & Osamu Miyawaki [2]

Earth's upper-level jet streams influence the speed and direction of travel of weather systems and commercial aircraft, and are linked to severe weather occurrence. Climate change is projected to accelerate the average upper-level jet stream winds. However, little is known about how fast (>99th percentile) upper-level jet stream winds will change. Here we show that fast upper-level jet stream winds get faster under climate change using daily data from climate model projections across a hierarchy of physical complexity. Fast winds also increase ~2.5 times more than the average wind response. We show that the multiplicative increase underlying the fast-get-faster response follows from the nonlinear Clausius–Clapeyron relation (moist-get-moister response). The signal is projected to emerge in both hemispheres by 2050 when considering scenario uncertainty. The results can be used to explain projected changes in commercial flight times, record-breaking winds, clear-air turbulence and a potential increase in severe weather occurrence under climate change.

Earth's jet streams are fast-flowing narrow bands of wind[1,2]. The fastest jet stream winds are eastward and occur in the upper troposphere ~10–12 km above the surface. Jet streams are important because they shape Earth's surface climate by steering weather systems and are linked to severe weather occurrence. In particular, the regions around fast upper-level jet stream winds (jet streaks) have been linked to the occurrence of severe storms, tornadoes, hail and severe wind[3–5]. Jet streams also affect the speed and path of commercial flights and can be responsible for clear-air turbulence[6,7]. The strength of the jet stream is influenced by different factors, including the thermal structure of the atmosphere and momentum transfer by weather systems (eddy-driven jet) and the tropical circulation (subtropical jet)[8–10].

Climate change is projected to accelerate the average upper-level jet stream winds following an increase in the meridional temperature gradient aloft[11–13]. The acceleration is projected to occur in both hemispheres. However, in the Northern Hemisphere it is weaker due to an opposing influence of Arctic amplification of surface temperature primarily during wintertime[10,14]. Consistent with the projected acceleration of the average upper-level jet stream winds, climate change is projected to significantly affect transatlantic flight times and increase clear-air turbulence[6,7].

In the literature, different changes in extremes under climate change have been documented. When the entire distribution shifts (for example, towards warmer temperature) then the extremes increase at the same rate as the average. This additive increase occurs for temperature extremes[15–18], although there can be regional exceptions. When the entire distribution increases by a fixed per cent then the extremes increase faster than the average. This multiplicative increase occurs for midlatitude precipitation extremes[19]. It is important to quantify how fast upper-level jet stream winds change under climate change and determine whether the response follows the average or not.

Little is known about how fast (>99th percentile) upper-level jet stream winds change under climate change. Changes in fast jet stream winds have important implications for commercial flight paths, clear-air turbulence and severe weather occurrence. Furthermore, no mechanism has been proposed to explain the response of fast jet stream winds. In contrast, there have been significant advances in our understanding of temperature and precipitation extremes, including the underlying physical mechanisms controlling their response to climate change[17–24]. Understanding the mechanisms controlling the climate change response is essential for having confidence in climate change projections[25,26].

[1]Department of the Geophysical Sciences, The University of Chicago, Chicago, IL, USA. [2]Climate and Global Dynamics Laboratory, National Center for Atmospheric Research, Boulder, CO, USA. e-mail: tas1@uchicago.edu

Here we quantify how fast upper-level jet stream winds, defined as days exceeding the 99th percentile of the daily distribution of 200 hPa zonal wind, change under climate change across a hierarchy of climate models from the World Climate Research Programme's Coupled Model Intercomparison Project Phase 6 (CMIP6)[27]. In order to quantify the response to anthropogenic forcing, we compare daily jet stream winds that exceed the 99th percentile at the end of the twentieth (1980–2000) and twenty-first (2080–2100) centuries under a high-emission scenario (Shared Socipeconomic Pathway (SSP) 5-8.5). When examining near-term trends, we also consider a lower-emission scenario (SSP2-4.5). The 200 hPa level is chosen following previous work[6]. Similar results are found for pressure levels around the cores of the upper-level jet streams (250 and 300 hPa) as discussed below.

Following previous work investigating precipitation extremes[20,21], we consider changes in fast upper-level jet stream winds as a function of latitude by aggregating data across all days and all longitudes at a given latitude. Thus, each longitudinal value is represented in the distribution. As the magnitude of extremes at a given percentile is known to depend on spatial resolution[28], we coarse-grain reanalysis data and use a common time frequency and spatial grid for reanalysis and climate model data to ensure a like-for-like comparison (Methods).

Fast jet stream winds exceed 60 m s^{-1} (134 mph) in the extratropics (20–60° latitude) of both hemispheres in reanalysis data[29] (dashed black line, Extended Data Fig. 1a). They occur throughout the seasonal cycle but are most common in the extended winter season (Supplementary Fig. 1). Climate models capture fast jet stream winds in reanalysis data reasonably well, including their latitudinal structure (compare black lines, Extended Data Fig. 1a). Fast winds exceed 75 m s^{-1} (168 mph) if the original reanalysis grid is used (Extended Data Fig. 1b).

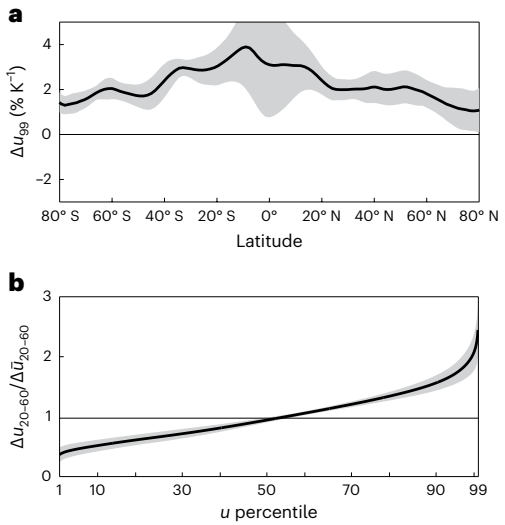

Fig. 1 | Fast jet stream winds under climate change. a, Fractional changes in fast (>99th percentile) 200 hPa jet stream winds normalized by the global mean change in surface air temperature (Δu_{99}) for each model. **b**, Response of the extratropical (20–60°) 200 hPa jet stream wind (Δu_{20-60}) in both hemispheres across percentiles relative to the response of the average wind ($\Delta\overline{u}_{20-60}$). The black horizontal line indicates the expected response following a uniform shift of the entire distribution towards faster wind. Data are presented as multi-model mean (thick line) ± one standard deviation of the response across the model ensemble (shading).

Fast upper-level jet stream winds get faster

Climate models project that fast upper-level jet stream winds get faster under climate change across the extratropics in both hemispheres by 2.1 ± 0.5% per degree of global mean change in surface air temperature, hereafter 2.1 ± 0.5% K^{-1} (mean ± s.d. across the climate model ensemble; Fig. 1a). Note each model response is calculated separately and normalized by its own global mean change in surface air temperature. We refer to this as the fast-get-faster response.

The fast-get-faster response under climate change occurs throughout the seasonal cycle (Extended Data Fig. 2), in the previous generation of coupled climate models[30] (Extended Data Fig. 3a) as well as in simpler models without coupling to the ocean or land (Extended Data Fig. 3b,c). It also occurs around the cores of the upper-level jet streams at 250 and 300 hPa (Extended Data Fig. 4), although the rate of increase is smaller. The smaller rate of increase may reflect the upward shift of the atmospheric circulation under climate change that has been connected to moist processes, in particular moist adiabatic adjustment[31]. The robustness of the fast-get-faster response suggests it is tied to a robust underlying physical mechanism.

The rate of increase of fast jet stream winds under climate change is close to the rate of increase of the average jet stream wind (2.6 ± 0.9% K^{-1}; Extended Data Fig. 5a). A similar multiplicative increase under climate change for the average and fast winds implies a change in the distribution. Consistently we find that the response of fast winds averaged across the extratropics increases substantially more than ~2.5 times the average wind response (Fig. 1b), whereas slow winds increase substantially less than ~0.5 times the average wind. Thus, the upper-level jet stream wind distribution involves a multiplicative increase (per cent increase) under climate change and not an additive increase (shift of the entire distribution) towards faster winds (Extended Data Fig. 6).

Previous work showed both the average upper-level jet stream wind and the vertical wind shear increase under climate change, consistent with an increase in the meridional temperature gradient[11,32,33]. Here we quantify the connection between changes in thermal structure under climate change and fast jet stream winds using thermal wind, u_T, which is defined as

$$u_T \equiv \int_{p_s}^{200\,\mathrm{hPa}} \frac{1}{fa}\frac{\partial \alpha(T,p)}{\partial \phi}\mathrm{d}p = \int_{p_s}^{200\,\mathrm{hPa}} \frac{R}{fap}\frac{\partial T}{\partial \phi}\mathrm{d}p \quad (1)$$

where p_s is surface pressure, f is the Coriolis parameter, a is the radius of Earth, $\alpha = 1/\rho$ is the specific volume where ρ is density, p is pressure, ϕ is latitude, R is the dry gas constant and T is the air temperature[2,8]. We neglect the surface wind in equation (1), which is small, consistent with previous work[33]. We use daily temperature data to compute u_T at each grid box and aggregate it across all days and all longitudes at a given latitude.

Thermal wind increases under climate change over the extratropics in both hemispheres by 2.1 ± 0.7% K^{-1} (Fig. 2a). The thermal wind response is significantly correlated with the fast-get-faster response across climate models (R = 0.90, P = 0.01). The slight deviation from a one-to-one relationship indicates that surface wind, ageostrophic processes such as friction and the numerical method used have a secondary influence. A similar relationship occurs for the average upper-level jet stream wind response (Extended Data Fig. 5b).

The robust relationship between the fast-get-faster response under climate change and thermal wind does not imply a causal understanding because temperature is influenced by many factors, including moisture[34,35], the atmospheric circulation[36], cloud radiative effects[37,38] and so on. To have confidence in the projected fast-get-faster response from climate models it is important to understand the mechanism underlying the ~2% K^{-1} rate of increase.

Fast-get-faster follows from moist-get-moister

A key factor that impacts the density and temperature responses, and thereby thermal wind, under climate change is moisture. Moisture exhibits two robust responses under climate change, which follow from the Clausius–Clapeyron relation provided there is a moisture source.

https://doi.org/10.1038/s41558-023-01884-1

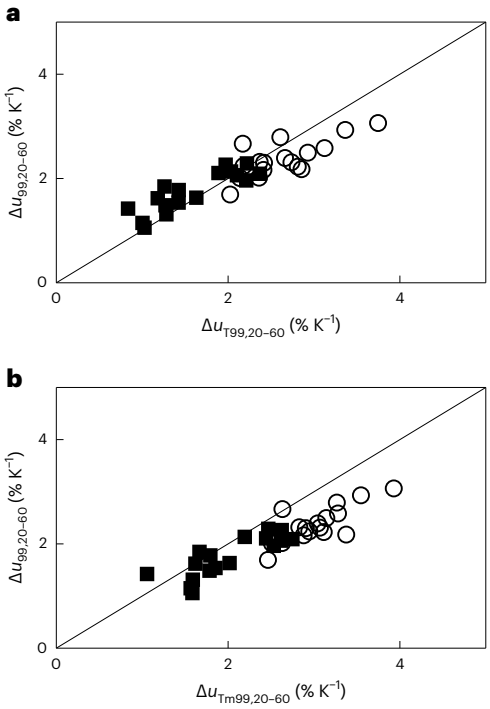

Fig. 2 | Relationship between fast jet stream winds and thermal wind. **a**,**b**, Fractional changes in fast (>99th percentile) 200 hPa jet stream winds averaged over the extratropics (20–60° latitude) normalized by the global mean change in surface air temperature for each model versus thermal wind (**a**; equation (1)) and moist thermal wind (**b**; equation (2)). Values from individual models for the Northern and Southern hemispheres are shown by squares and circles, respectively.

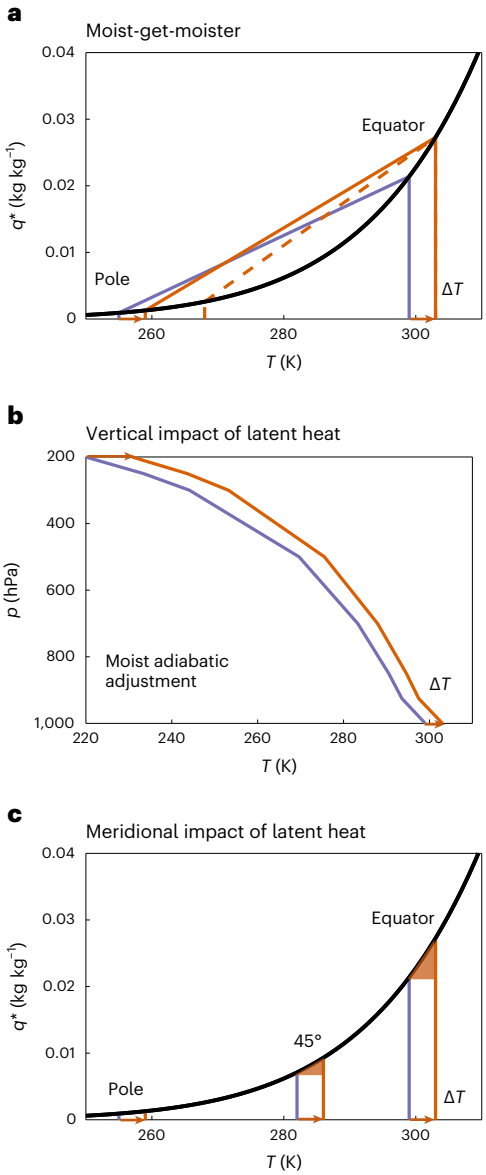

Fig. 3 | Robust responses of moisture under climate change following the Clausius–Clapeyron relation. **a**, Moist-get-moister response involves warmer air 'holding' more moisture following the Clausius–Clapeyron relation (black line), with the largest increase near the Equator. It implies an increased meridional gradient of saturation specific humidity under uniform warming (slopes of blue versus orange lines) and polar-amplified warming (compare *y*-axis range of solid blue and dashed orange lines). **b**, Latent heat release aloft by rising air parcels that 'hold' more moisture following moist adiabatic adjustment under climate change (uniform surface warming indicated from blue to orange). **c**, The latent heat release aloft (orange triangle) is largest at the Equator following the Clausius–Clapeyron relation (black line).

The first response involves an increase of saturation specific humidity with temperature[39], which follows from the Clausius–Clapeyron relation (black line, Fig. 3a). The increase involves warmer air 'holding' more moisture via evaporation at all latitudes, with the largest increase near the Equator. The consequence is an increase of the meridional gradient of saturation specific humidity between the Equator and the pole under uniform global warming (compare slopes of solid blue and orange lines, Fig. 3a) and polar-amplified warming projected by climate models (compare *y*-axis range of solid blue and dashed orange lines, Fig. 3a). We refer to this as moist-get-moister. Ultimately, it implies an increase in the meridional density gradient (adding water vapour to an air parcel at roughly the same temperature and pressure makes it lighter, because the molecular mass of dry air is 29 g mol^{-1} whereas that of water vapour is 18 g mol^{-1})[40,41] and can thereby affect thermal wind and the jet stream. Previous work showed vertically integrated specific humidity[39] and the meridional gradient of near-surface specific humidity[42,43] both increase under climate change following the Clausius–Clapeyron relation.

The second response involves latent heat release (condensation) by rising air parcels that 'hold' more moisture following the Clausius–Clapeyron relation. The additional latent heat is released aloft, leading to amplified warming aloft and a weakened vertical temperature gradient (Fig. 3b) under climate change[34,35,44]. We refer to this as moist adiabatic adjustment. Latent heat release also varies meridionally: it is larger for rising parcels (either upright or slantwise) near the Equator than those in the extratropics or polar region (orange triangles, Fig. 3c). Note the latent heat release response involves the moist-get-moister response but in addition requires rising air parcels and condensation. Thus, it is related to the wet-get-wetter or rich-get-richer response of precipitation (precipitation is the vertical integral of latent heat release) under climate change, which is affected by moist-get-moister and convective mass flux responses[39,45]. Previous work showed the latent heat release response is important in the extratropics under climate change. In particular, extratropical dry entropy increases aloft under climate change due to warming aloft. However, the vertical gradient of saturated equivalent potential temperature (moist static stability) is largely unchanged, consistent with the impact of latent heat release from moist adiabatic adjustment[46]. This is consistent with the importance of moisture for the climatological static stability of the extratropical atmosphere[47–49].

https://doi.org/10.1038/s41558-023-01884-1

To understand the fast-get-faster response and its connection to moisture under climate change, we consider moist thermal wind, u_{Tm}, which is defined as

$$u_{\mathrm{Tm}} \equiv \int_{p_s}^{200\,\mathrm{hPa}} \frac{1}{fa}\frac{\partial \alpha(s^*,p)}{\partial \phi}\mathrm{d}p = \int_{p_s}^{200\,\mathrm{hPa}} \frac{1}{fa}\left(\frac{\partial T}{\partial p}\right)_{s^*}\frac{\partial s^*}{\partial \phi}\mathrm{d}p \qquad (2)$$

where $(\partial T/\partial p)_{s^*}$ is the moist adiabatic lapse rate in pressure coordinates, $s^* = c_p \ln\theta_e^*$ is the saturation (moist) entropy, c_p is the specific heat of air at constant pressure and θ_e^* is the equivalent potential temperature air would have if it were saturated at the same temperature and pressure. Saturation entropy is the sum of dry entropy ($s_d = c_p \ln\theta$, where θ is potential temperature) and saturation specific humidity (q^*), that is, $s^* = s_d + L_v q^*/T$, where L_v is the latent heat of vaporization. Moist thermal wind can be derived by writing the specific volume α as a function of s^* and p and using a thermodynamic Maxwell relation (Methods)[50,51].

Moist thermal wind can be used to understand how the fast-get-faster response under climate change is influenced by the response of moisture. In particular, the response of moist thermal wind under climate change is

$$\Delta u_{\mathrm{Tm}} \approx \frac{1}{fa}\int_{p_s}^{200\,\mathrm{hPa}} \left[\underbrace{\frac{\partial s^*}{\partial \phi}\Delta\left(\frac{\partial T}{\partial p}\right)_{s^*}}_{\text{Moist adiabatic adjustment}} + \left(\frac{\partial T}{\partial p}\right)_{s^*}\Delta\left(\frac{\partial s^*}{\partial \phi}\right)\right]\mathrm{d}p + \text{residual} \qquad (3)$$

where Δ is the difference between the end of the twenty-first and twentieth centuries. The residual is small, confirming the usefulness of the moist thermal wind decomposition (Extended Data Fig. 7).

The first term on the right-hand side of equation (3) quantifies the impact of latent heat release following moist adiabatic adjustment (Fig. 3b). The second term on the right-hand side of equation (3) depends on the meridional gradient of dry entropy (s_d), which is affected by meridionally varying latent heat release (Fig. 3c), and the meridional gradient of saturation specific humidity (q^*), which quantifies the moist-get-moister response (Fig. 3a), that is

$$\Delta\left(\frac{\partial s^*}{\partial \phi}\right) = \underbrace{\Delta\left(\frac{\partial s_d}{\partial \phi}\right)}_{\text{Dry entropy gradient}} + \underbrace{\Delta\left(\frac{\partial}{\partial \phi}\left(\frac{L_v q^*}{T}\right)\right)}_{\text{Moist-get-moister}} \qquad (4)$$

thus

$$\Delta u_{\mathrm{Tm}} \approx \frac{1}{fa}\int_{p_s}^{200\,\mathrm{hPa}} \left[\underbrace{\frac{\partial s^*}{\partial \phi}\Delta\left(\frac{\partial T}{\partial p}\right)_{s^*}}_{\text{Moist adiabatic adjustment}} + \underbrace{\left(\frac{\partial T}{\partial p}\right)_{s^*}\Delta\left(\frac{\partial s_d}{\partial \phi}\right)}_{\text{Dry entropy gradient}} + \underbrace{\left(\frac{\partial T}{\partial p}\right)_{s^*}\Delta\left(\frac{\partial}{\partial \phi}\left(\frac{L_v q^*}{T}\right)\right)}_{\text{Moist-get-moister}}\right]\mathrm{d}p. \qquad (5)$$

We use daily temperature data to compute moist thermal wind u_{Tm} at each grid box and aggregate it across all days and all longitudes at a given latitude. Moist thermal wind increases under climate change over the extratropics in both hemispheres by 2.5 ± 0.6% K^{-1} (Fig. 2b) and the response is significantly correlated with the fast-get-faster response across climate models ($R = 0.89$, $P = 0.01$). A similar relationship occurs for the average jet stream wind (Extended Data Fig. 5c).

The moist-get-moister response increases the meridional gradient of saturation specific humidity (Fig. 3a and third term on right-hand side of equation (5)) and thereby increases moist thermal wind (orange line, Fig. 4a). More specifically, it contributes to an increase of 2.2 ± 0.2% K^{-1} averaged over the extratropics. The moist-get-moister response also leads to fast winds getting faster than the average wind (orange line, Fig. 4b) under climate change.

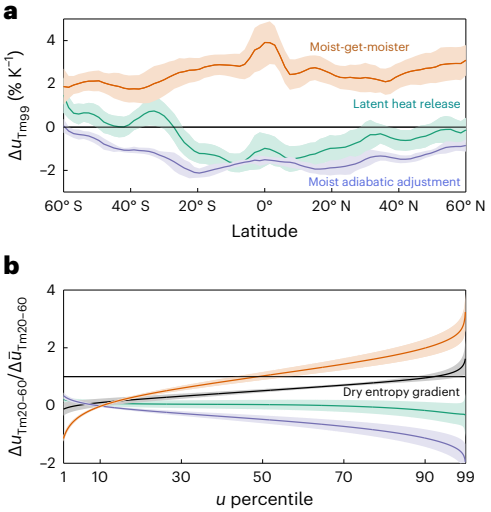

Fig. 4 | Relationship between fast jet stream winds and moisture under climate change. a, Fractional changes in fast (>99th percentile) moist thermal wind (Δu_{Tm99}) due to the contributions from moist-get-moister, latent heat release and moist adiabatic adjustment responses (see equation (5)) normalized by the global mean change in surface air temperature for each model. **b**, Response of moist thermal wind over the extratropics (20–60° latitude, $\Delta u_{\mathrm{Tm20-60}}$) in both hemispheres across percentiles relative to the response of the average wind ($\Delta\bar{u}_{\mathrm{Tm20-60}}$) due to the contributions in **a** and dry entropy responses (see equation (5)). Data are presented as multi-model mean (thick line) ± one standard deviation of the response across the model ensemble (shading).

The moist-get-moister response can be affected by a change in the meridional temperature gradient (dashed orange line, Fig. 3a). The impact of the meridional temperature gradient response can be quantified by imposing only the change in global mean temperature between the twenty-first and twentieth centuries, that is, $T_{21\mathrm{st}^*}(\lambda,\phi,p,t) = T_{20\mathrm{th}}(\lambda,\phi,p,t) + \Delta T_{\mathrm{gm}}(p)$, where $T_{20\mathrm{th}}$ and $T_{21\mathrm{st}}$ refer to the twentieth- and twenty-first-century temperature, respectively, λ is longitude, and ΔT_{gm} is the change in global mean temperature, which only depends on pressure. Imposing $T_{21\mathrm{st}^*}$ is analogous to the moist-get-moister response under uniform global warming (compare solid blue and orange lines, Fig. 3a). The moist-get-moister response to meridionally uniform global warming leads to an increase of moist thermal wind (2.0 ± 0.6% K^{-1}; Extended Data Fig. 8a), which is very similar to the response to meridionally varying warming. Furthermore, the moist-get-moister response with no change in meridional temperature gradient also leads to fast winds getting faster than the average wind under climate change (Extended Data Fig. 8b). This implies that the moist-get-moister response is fundamentally tied to the climatological (twentieth-century) meridional temperature gradient and the nonlinear Clausius–Clapeyron relation. The small impact of the meridional temperature gradient response on the moist-get-moister response is consistent with the dominance of saturation specific humidity changes over temperature changes, that is,

$$\Delta\left(\frac{\partial}{\partial \phi}\left(\frac{L_v q^*}{T}\right)\right) = \frac{L_v q^*}{T}\left[\frac{1}{q^*}\frac{\partial \Delta q^*}{\partial \phi} - \frac{1}{T}\frac{\partial \Delta T}{\partial \phi}\right] \approx \frac{L_v}{T}\frac{\partial \Delta q^*}{\partial \phi} \qquad (6)$$

because $\Delta q^*/q^* \approx 28\% > \Delta T/T \approx 1\%$, following Fig. 3a.

The remaining two terms in the moist thermal wind decomposition, which are affected by latent heat release, namely moist adiabatic adjustment and the meridional dry entropy gradient, lead to a small response (the sum of first and second terms on the right-hand side of equation (5); green line, Fig. 4a). More specifically, together they

https://doi.org/10.1038/s41558-023-01884-1

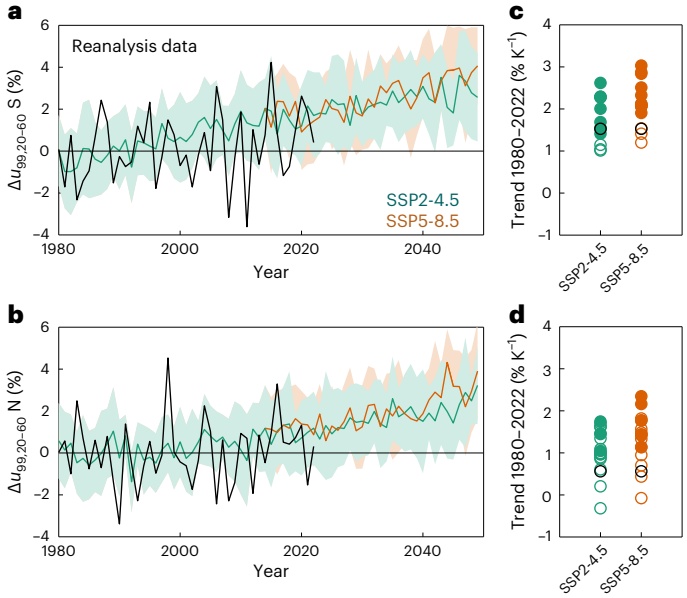

Fig. 5 | Emergence of fast-get-faster signal. a,**b**, Time series of fractional changes (relative to the 1980–2000 period) in fast 200 hPa jet stream winds in reanalysis and climate models for different emission scenarios for the Southern (**a**) and Northern (**b**) Hemisphere extratropics in the satellite era (1980–2022). Data are presented as multi-model mean (thick line) ± one standard deviation of the response across the model ensemble (shading). **c**,**d**, Linear trends of fractional changes in fast jet stream winds in reanalysis and climate models for different scenarios normalized by the global mean warming of surface air temperature for each dataset in the Southern (**c**) and Northern (**d**) Hemisphere extratropics. Statistically significant trends are indicated by closed circles.

contribute to a change of 0.2 ± 0.7% K^{-1} averaged over the extratropics and also lead to a small change in the wind distribution (green line, Fig. 4b). The small response is the result of opposing influences of latent heat release associated with moist adiabatic adjustment, which decreases moist thermal wind (blue line, Fig. 4a), and the meridional dry entropy gradient, which increases moist thermal wind (difference between blue and green lines, Fig. 4a). Neither contribution can account for fast winds getting significantly faster than the average (blue and black lines, Fig. 4b).

Why do fast winds get faster? Taken all together, the moist thermal wind decomposition shows we can understand the fast-get-faster response of the upper-level jet stream winds under climate change from the moist-get-moister response, that is, the increased meridional saturation specific humidity gradient under climate change, that follows from the nonlinear Clausius–Clapeyron relation (Fig. 3a). The moist-get-moister response involves evaporation not latent heat release and increases thermal wind by increasing the meridional density gradient. Interestingly, the rate of increase of the fast-get-faster response (~2% K^{-1}) is close to the rate of increase of evaporation under climate change ~2% K^{-1} (refs. 39,52). The other effects of moisture, which involve latent heat release (moist adiabatic adjustment and increased meridional dry entropy gradient), oppose one another. More specifically, the latent heat release contribution exhibits a dipole vertical structure (Supplementary Fig. 2a). The latent heat release dipole is consistent with its role in producing an upward shift of the atmospheric circulation under climate change[31] and it being more important at 250 hPa and 300 hPa (green lines, Extended Data Fig. 9). The dry entropy gradient dominates above 400 hPa (Supplementary Fig. 2b), consistent with enhanced tropical upper tropospheric warming and extratropical stratospheric cooling[35,46], and contributes to the larger response of fast winds at 200 hPa. A similar mechanistic understanding holds for the response of the average jet stream wind (Extended Data Fig. 10) under climate change. Hence, the moist-get-moister response can also explain why fast jet stream winds increase substantially more than the average wind, that is, why the increase is multiplicative rather than additive.

Emergence of fast-get-faster signal

The fast-get-faster response under climate change is robust across the extratropics between the end of the twenty-first and twentieth centuries under the SSP5-8.5 scenario (Fig. 1a). Over the satellite era (1980–2022), linear trends in fast upper-level jet stream winds across the extratropics are positive in reanalysis data (black lines, Fig. 5a,b), but the linear trend coefficients are not statistically significant ($P = 0.14$ for the Southern Hemisphere, $P = 0.42$ for the Northern Hemisphere; open black circles, Fig. 5c,d). The linear trends of fast jet stream winds over the satellite era in climate models under the SSP2-4.5 and SSP5-8.5 scenarios exhibit considerable spread (green and orange shading, Fig. 5a,b), with some models having insignificant linear trends (open coloured circles, Fig. 5c,d).

When fast upper-level jet stream wind trends over the satellite era are weighted by global mean surface air temperature trends, the reanalysis trends fall within the distribution of climate model trends in both hemispheres (Fig. 5c,d). However, the reanalysis trends are on the low end of the model trend distribution, which is consistent with climate models exhibiting stronger tropical upper tropospheric warming trends than observations[53]. Given the spread in the climate model trends, we use the model distribution to characterize the emergence of the fast-get-faster signal by calculating the year when all models in the ensemble project a statistically significant linear trend for the time series beginning in 1980. All climate models in the ensemble project a statistically significant fast-get-faster signal (P value of linear trend coefficient for each model is <0.05) across the Southern and Northern Hemisphere extratropics by 2035 and 2045, respectively, following the SSP5-8.5 scenario. Following the SSP2-4.5 scenario, all climate models in the ensemble project a statistically significant fast-get-faster signal across the Southern and Northern Hemisphere extratropics by 2038 and 2048. Thus, the fast-get-faster signal is projected to emerge in both hemispheres by 2050.

Discussion

We have shown, using daily data from climate model projections across a hierarchy of physical complexity, that fast upper-level jet stream winds get faster under climate change. In addition, fast winds increase ~2.5 times more than the average wind response; thus climate models project record-breaking upper-level jet stream winds in the future. We provide a physical basis for the fast-get-faster response and show that the multiplicative increase is consistent with the moist-get-moister response (increased meridional saturation specific humidity gradient under climate change) that follows from the nonlinear Clausius–Clapeyron relation. The moist-get-moister response involves evaporation not latent heat release, and impacts thermal wind directly through the meridional density gradient. The results show that moist processes can be used to understand the response of extratropical jet stream winds under climate change, including fast jet stream winds. Furthermore, the robustness of the physical mechanism underlying the fast-get-faster response and the fact it occurs across a climate model hierarchy gives confidence in climate model projections. While the fast-get-faster signal has not emerged in reanalysis data, the signal is projected to emerge in both hemispheres by 2050 when considering scenario uncertainty. Finally, the results can be used to explain the significant projected changes in commercial flight times and clear-air turbulence in the future. They also point to a critical need to understand the impact of the fast-get-faster response for severe weather occurrence in the future.

Online content

Any methods, additional references, Nature Portfolio reporting summaries, source data, extended data, supplementary information, acknowledgements, peer review information; details of author contributions and competing interests; and statements of data and code availability are available at https://doi.org/10.1038/s41558-023-01884-1.

References

1. Wallace, J. M. & Hobbs, P. V. *Atmospheric Science: An Introductory Survey* (Academic Press, 2006).
2. Holton, J. M. & Hakim, G. *An Introduction to Dynamic Meteorology* (Academic Press, 2012).
3. McNulty, R. P. On upper tropospheric kinematics and severe weather occurence. *Mon. Weather Rev.* **106**, 662–672 (1978).
4. Rose, S. F., Hobbs, P. V., Locatelli, J. D. & Stoelinga, M. T. A 10-yr climatology relating the locations of reported tornadoes to the quadrants of upper-level jet streaks. *Weather Forecast.* **119**, 301–309 (2004).
5. Clark, A. J., Schaeffer, C. J., Gallus, W. A. Jr & Johnson-O'Mara, K. Climatology of storm reports relative to upper-level jet streaks. *Weather Forecast.* **24**, 1032–1051 (2009).
6. Williams, P. D. Transatlantic flight times and climate change. *Environ. Res. Lett*. https://doi.org/10.1088/1748-9326/11/2/024008 (2016).
7. Williams, P. D. & Joshi, M. M. Intensification of winter transatlantic aviation turbulence in response to climate change. *Nat. Clim. Change* https://doi.org/10.1038/nclimate1866 (2013).
8. Vallis, G. K. *Atmospheric and Oceanic Fluid Dynamics Fundamentals and Large-scale Circulation* (Cambridge Univ. Press, 2006).
9. Schneider, T. The general circulation of the atmosphere. *Annu. Rev. Earth Planet. Sci.* **34**, 655–688 (2006).
10. Shaw, T. A. et al. Storm track processes and the opposing influences of climate change. *Nat. Geosci*. https://doi.org/10.1038/NGEO2783 (2016).
11. Lorenz, D. J. & DeWeaver, E. T. Tropopause height and zonal wind response to climate change in the IPCC scenario integrations. *J. Geophys. Res*. https://doi.org/10.1029/2006JD008087 (2007).
12. Stendel, M., Francis, J., White, R., Williams, P. D. & Woollings, T. in *Climate Change: Observed Impacts on Planet Earth* 3rd edn (ed. Letcher, T. M.) Ch. 15 (Elsevier, 2021).
13. Woollings, T., Drouard, M., O'Reilly, C. H., Sexton, D. M. H. & McSweeney, C. Trends in the atmospheric jet streams are emerging in observations and could be linked to tropical warming. *Commun. Earth Environ*. https://doi.org/10.1038/s43247-023-00792-8 (2023).
14. Barnes, E. A. & Screen, J. The impact of Arctic warming on the midlatitude jet stream: Can it? Has it? Will it? *Wiley Interdiscip. Rev. Clim. Change* **6**, 277–286 (2015).
15. Rhines, A. & Huybers, P. Frequent summer temperature extremes reflect changes in the mean, not the variance. *Proc. Natl Acad. Sci. USA* https://doi.org/10.1073/pnas.1218748110 (2013).
16. Rey, J., Rohat, G., Perroud, M., Goyette, S. & Kasparian, J. Shifting velocity of temperature extremes under climate change. *Environ. Res. Lett*. https://doi.org/10.1088/1748-9326/ab6c6f (2020).
17. Horton, R. M., Mankin, J. S., Lesk, C., Coffel, E. & Raymond, C. A review of recent advances in research on extreme heat events. *Curr. Clim. Change Rep.* **2**, 242–259 (2016).
18. Garfinkel, C. & Harnik, N. The non-Gaussianity and spatial asymmetry of temperature extremes relative to the storm track: the role of horizontal advection. *J. Clim.* **30**, 445–464 (2017).
19. O'Gorman, P. A. Precipitation extremes under climate change. *Curr. Clim. Change Rep.* **1**, 49–59 (2015).
20. O'Gorman, P. A. & Schneider, T. The physical basis for increases in precipitation extremes in simulations of 21st-century climate change. *Proc. Natl Acad. Sci. USA* **106**, 14773–14777 (2009).
21. O'Gorman, P. A. & Schneider, T. Scaling of precipitation extremes over a wide range of climates simulated with an idealized GCM. *J. Clim.* **22**, 5676–5685 (2009).
22. Byrne, M. P. Amplified warming of extreme temperatures over tropical land. *Nat. Geosci.* **14**, 837–841 (2021).
23. Zhang, Y., Held, I. M. & Fueglistaler, S. Projections of tropical heat stress constrained by atmospheric dynamics. *Nat. Geosci.* **14**, 133–137 (2021).
24. Zhang, Y. & Boos, W. R. An upper bound for extreme temperatures over midlatitude land. *Proc. Natl Acad. Sci. USA* https://doi.org/10.1073/pnas.2215278120 (2023).
25. Held, I. M. The gap between simulation and understanding in climate modeling. *Bull. Am. Meteorol. Soc*. https://doi.org/10.1175/BAMS-86-11-1609 (2005).
26. Shaw, T. A. Mechanisms of future predicted changes in the zonal mean midlatitude circulation. *Curr. Clim. Change Rep.* **5**, 345–357 (2019).
27. Eyring, V. Overview of the Coupled Model Intercomparison Project Phase 6 (CMIP6) experimental design and organization. *Geosci. Model Dev.* **9**, 1937–1958 (2016).
28. Chen, C. T. & Knutson, T. On the verification and comparison of extreme rainfall indices from climate models. *J. Clim.* **21**, 1605–1621 (2008).
29. Hershbach, H. et al. The ERA5 global reanalysis. *Q. J. R. Meteorol. Soc*. https://doi.org/10.1002/qj.3803 (2020).
30. Taylor, K. E., Stouffer, R. J. & Meehl, G. A. An overview of CMIP5 and the experiment design. *Bull. Am. Meteorol. Soc*. https://doi.org/10.1175/BAMS-D-11-00094.1 (2012).
31. Singh, M. S. & O'Gorman, P. A. Upward shift of the atmospheric general circulation under global warming: theory and simulations. *J. Clim.* **25**, 8259–8276 (2012).
32. Allen, R. J. & Sherwood, S. C. Warming maximum in the tropical upper troposphere deduced from thermal winds. *Nat. Geosci.* **1**, 399–403 (2008).
33. Lee, S., Williams, P. D. & Frame, T. Increased shear in the North Atlantic upper-level jet stream over the past four decades. *Nature* **572**, 639–642 (2019).
34. Held, I. M. Large-scale dynamics and global warming. *Bull. Am. Meteorol. Soc*. **74**, 228–242 (1993).
35. Vallis, G. K., Zurita-Gotor, P., Cairns, C. & Kidston, J. Response of the large-scale structure of the atmosphere to climate change. *Q. J. R. Meteorol. Soc*. **141**, 1479–1501 (2015).
36. Wu, Y., Seager, R., Ting, M., Naik, N. & Shaw, T. A. Atmospheric circulation response to an instantaneous doubling of carbon dioxide. Part I: model experiments and transient thermal response in the troposphere. *J. Clim.* **25**, 2862–2879 (2012).
37. Voigt, A. & Shaw, T. A. Circulation response to warming shaped by radiative changes of clouds and water vapour. *Nat. Geosci*. https://doi.org/10.1038/NGEO2345 (2015).
38. Ceppi, P. & Hartmann, D. L. Clouds and the atmospheric circulation response to warming. *J. Clim.* **29**, 783–799 (2016).
39. Held, I. M. & Soden, B. J. Robust responses of the hydrological cycle to global warming. *J. Clim.* **19**, 5686–5699 (2006).
40. Emanuel, K. A. *Atmospheric Convection* (Oxford Univ. Press, 1994).
41. Yang, D. & Seidel, S. D. The incredible lightness of water vapor. *J. Clim.* **33**, 2841–2851 (2020).
42. Shaw, T. A. & Voigt, A. What can moist thermodynamics tell us about circulation shifts in response to uniform warming? *Geophys. Res. Lett*. https://doi.org/10.1002/2016GL068712 (2016).
43. Tan, Z. & Shaw, T. A. Quantifying the impact of wind and surface humidity-induced surface heat exchange on the circulation shift in response to increased CO_2. *Geophys. Res. Lett*. https://doi.org/10.1029/2020GL088053 (2020).

44. Miyawaki, O., Tan, Z., Shaw, T. A. & Jansen, M. F. Quantifying key mechanisms that contribute to the deviation of the tropical warming profile from a moist adiabat. *Geophys. Res. Lett*. https://doi.org/10.1029/2020GL089136 (2020).
45. Chou, C. & Neelin, J. D. Mechanisms of global warming impacts on regional tropical precipitation. *J. Clim*. **17**, 2688–2701 (2004).
46. Frierson, D. M. W. Robust increases in midlatitude static stability in simulations of global warming. *Geophys. Res. Lett*. https://doi.org/10.1029/2006GL027504 (2006).
47. Juckes, M. N. The static stability of the midlatitude troposphere: the relevance of moisture. *J. Atmos. Sci*. **57**, 3050–3057 (2000).
48. Korty, R. & Schneider, T. A climatology of the tropospheric thermal stratification using saturation potential vorticity. *J. Clim*. **20**, 5977–5991 (2007).
49. Wu, Y. & Pauluis, O. Midlatitude tropopause and low-level moisture. *J. Atmos. Sci*. **71**, 1187–1200 (2014).
50. Emanuel, K. A. An air–sea interaction theory for tropical cyclones. Part I. *J. Atmos. Sci*. **43**, 585–604 (1986).
51. Emanuel, K. A. On thermally direct circulation in moist atmospheres. *J. Atmos. Sci*. **52**, 1529–1534 (1995).
52. Schneider, T., O'Gorman, P. A. & Levine, X. Water vapor and the dynamics of climate changes. *Rev. Geophys*. https://doi.org/10.1029/2009RG000302 (2010).
53. Po-Chedley, S. et al. Internal variability and forcing influence model–satellite differences in the rate of tropical tropospheric warming. *Proc. Natl Acad. Sci. USA* https://doi.org/10.1073/pnas.2209431119 (2022).

Methods

Reanalysis and climate model data

We use daily zonal wind (variable ua), atmospheric temperature (variable ta) and surface air temperature (variable tas) data from 18 CMIP6 (Supplementary Table 1) and 18 CMIP5 (Supplementary Table 2) models. We also use daily zonal wind data from the ECMWF Reanalysis v5 (ERA5) reanalysis from 1980 to 2022. For ERA5, the daily zonal wind data was constructed from hourly data.

The magnitude of extremes at a given percentile is known to depend on spatial resolution[28]. To ensure a like-for-like comparison, we examine the reanalysis and climate model extremes on the same spatial grid. For the vertical grid, we interpolate all daily data onto a common vertical grid with 12 pressure levels (1,000, 925, 850, 700, 500, 300, 250, 200, 150, 100, 50 and 10 hPa) using log interpolation. The 37-pressure-level reanalysis data are sub-sampled onto the same 8-pressure-level climate model vertical grid before interpolating. For the horizontal grid, we interpolate all data onto a 1.5° × 1.5° grid using cubic spline interpolation. Coarse-graining the reanalysis data leads to weaker extremes consistent with previous analysis of precipitation extremes (Extended Data Fig. 1).

Statistical tests

The statistical significance of the relationship between zonal wind and thermal wind responses across models for both hemispheres (Fig. 2) is quantified by the P value of the Pearson's correlation coefficient according to a two-tailed t-test.

The satellite-era trends (Fig. 5) were quantified by a least-squares linear regression model. The statistical significance of the linear trend was assessed at the 95% confidence level (P value of the linear coefficient of the least-squares linear regression model <0.05) according to a two-tailed t-test. In addition, a Durbin–Watson test was performed to test the autocorrelation of the residuals of the linear regression model and the statistical significance of the Durbin–Watson test was computed following ref. 54. The results of the Durbin–Watson test show the autocorrelation is not significant. In particular, for the reanalysis trends the Durbin–Watson P values are $P = 0.91$ for the Southern Hemisphere and $P = 0.93$ for the Northern Hemisphere. The Durbin–Watson P values for the climate model ensemble mean trends are $P = 0.58$ for the Southern Hemisphere and $P = 0.50$ for the Northern Hemisphere. These large P values ($P > 0.05$) indicate we can confirm the null hypothesis that the autocorrelation of the residuals is not significant.

Moist thermal wind

Moist thermal wind can be derived for a saturated atmosphere by writing the specific volume $\alpha = \alpha(s^*, p)$, where s^* is the saturated moist entropy, which is conserved under moist reversible processes, and p is pressure[50,51]. The meridional gradient of specific volume, which appears in the equation for thermal wind (equation (2)), can be written as

$$\left(\frac{\partial \alpha}{\partial \phi}\right)_p = \left(\frac{\partial \alpha}{\partial s^*}\right)_p \frac{\partial s^*}{\partial \phi}. \tag{7}$$

Saturated moist entropy satisfies the first law of thermodynamics

$$T\mathrm{d}s^* = \mathrm{d}u + p\mathrm{d}\alpha - L\mathrm{d}q^* \tag{8}$$

which can be written as a function of saturated moist enthalpy $h^* \equiv u + p\alpha - Lq^*$ such that

$$\mathrm{d}h^* = T\mathrm{d}s^* + \alpha\mathrm{d}p. \tag{9}$$

These relationships imply

$$\left(\frac{\partial h^*}{\partial p}\right)_{s^*} = \alpha \tag{10}$$

$$\left(\frac{\partial h^*}{\partial s^*}\right)_p = T. \tag{11}$$

Because $q^*(T, p)$ and $h^*(s^*, p)$, we have equality of mixed partial derivatives

$$\left(\frac{\partial}{\partial s^*}\right)_p \left(\frac{\partial h^*}{\partial p}\right)_{s^*} = \left(\frac{\partial}{\partial p}\right)_{s^*} \left(\frac{\partial h^*}{\partial s^*}\right)_p \tag{12}$$

and upon substitution into equations (9) and (10) we obtain the Maxwell relation

$$\left(\frac{\partial \alpha}{\partial s^*}\right)_p = \left(\frac{\partial T}{\partial p}\right)_{s^*} \tag{13}$$

where the right-hand side is the moist adiabatic lapse rate. The meridional gradient of specific volume is

$$\left(\frac{\partial \alpha}{\partial \phi}\right)_p = \left(\frac{\partial T}{\partial p}\right)_{s^*} \frac{\partial s^*}{\partial \phi}. \tag{14}$$

This becomes moist thermal wind upon substitution of $(\partial\alpha/\partial\phi)_p$ into the thermal wind equation:

$$u_{\mathrm{Tm}} \equiv \int_{p_s}^{200\,\mathrm{hPa}} \frac{1}{fa} \frac{\partial \alpha(s^*, p)}{\partial \phi} \mathrm{d}p = \int_{p_s}^{200\,\mathrm{hPa}} \frac{1}{fa} \left(\frac{\partial T}{\partial p}\right)_{s^*} \frac{\partial s^*}{\partial \phi} \mathrm{d}p. \tag{15}$$

The physical interpretation of moist thermal wind is that changes in the meridional density gradient in a moist atmosphere can be influenced by changes the meridional gradient of saturation entropy and the impact of latent heat release aloft via the moist adiabatic lapse rate.

Data availability

The data used in the paper are publicly available: CMIP6 (https://esgf-node.llnl.gov/projects/cmip6/), CMIP5 (https://esgf-node.llnl.gov/projects/cmip5/) and ERA5 (https://cds.climate.copernicus.eu/cdsapp#!/dataset/reanalysis-era5-pressure-levels?tab=overview).

Code availability

The codes used in the manuscript are available at https://doi.org/10.5281/zenodo.8428075 (ref. 55).

References

54. Farebrother, R. W. Pan's procedure for the tail probabilities of the Durbin–Watson statistic. *Appl. Stat.* **29**, 224–227 (1980).
55. Shaw, T. A. Fast upper-level jet stream winds get faster under climate change. *Zenodo* https://doi.org/10.5281/zenodo.8428075 (2023).

Acknowledgements

This work was completed in part with resources provided by the University of Chicago's Research Computing Center. We acknowledge the World Climate Research Programme's Working Group on Coupled Modelling, which is responsible for CMIP, and we thank the climate modelling groups listed in Supplementary Table 1 for producing and making available their model output. For CMIP, the US Department of Energy's Program for Climate Model Diagnosis and Intercomparison provides coordinating support and led development of software infrastructure in partnership with the Global Organization for Earth System Science Portals.

Author contributions

T.A.S. conceived the study and analysed the data. O.M. acquired the data. Both authors discussed the results and wrote the paper.

Competing interests
The authors declare no competing interests.

Additional information
Extended data is available for this paper at https://doi.org/10.1038/s41558-023-01884-1.

Supplementary information The online version contains supplementary material available at https://doi.org/10.1038/s41558-023-01884-1.

Correspondence and requests for materials should be addressed to Tiffany A. Shaw.

Peer review information *Nature Climate Change* thanks Panos Athanasiadis and the other, anonymous, reviewer(s) for their contribution to the peer review of this work.

https://doi.org/10.1038/s41558-023-01884-1

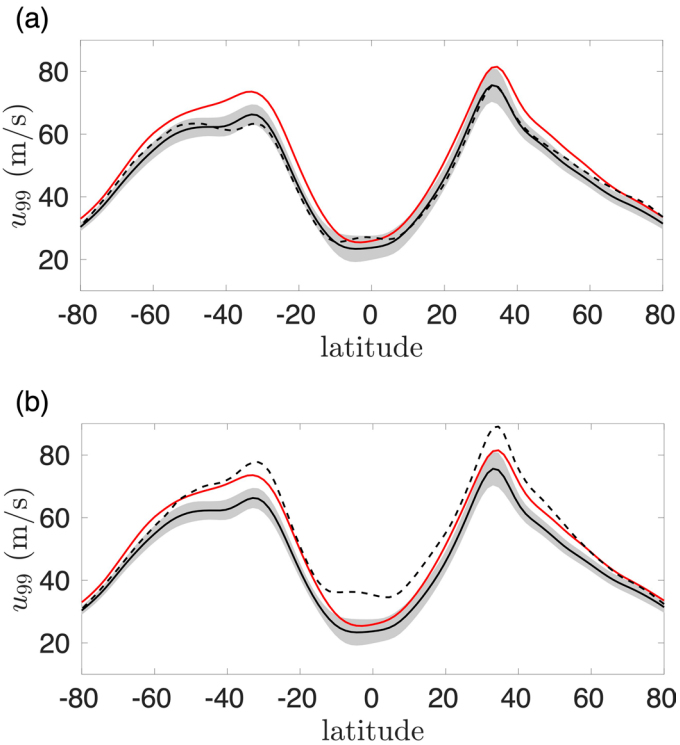

Extended Data Fig. 1 | Fast jet stream winds in reanalysis data and climate models. The fast (> 99th percentile) daily upper-level (200 hPa) jet stream (zonal) winds for historical (1980 to 2000, black) and future (2080 to 2100, red) climates for coupled climate models (solid) and reanalysis data (dashed) on (a) coarse-grained grid (see Methods) and (b) original grid. Data are presented as multi-model-mean (thick line) ± one standard deviation of the response across the model ensemble (shading).

https://doi.org/10.1038/s41558-023-01884-1

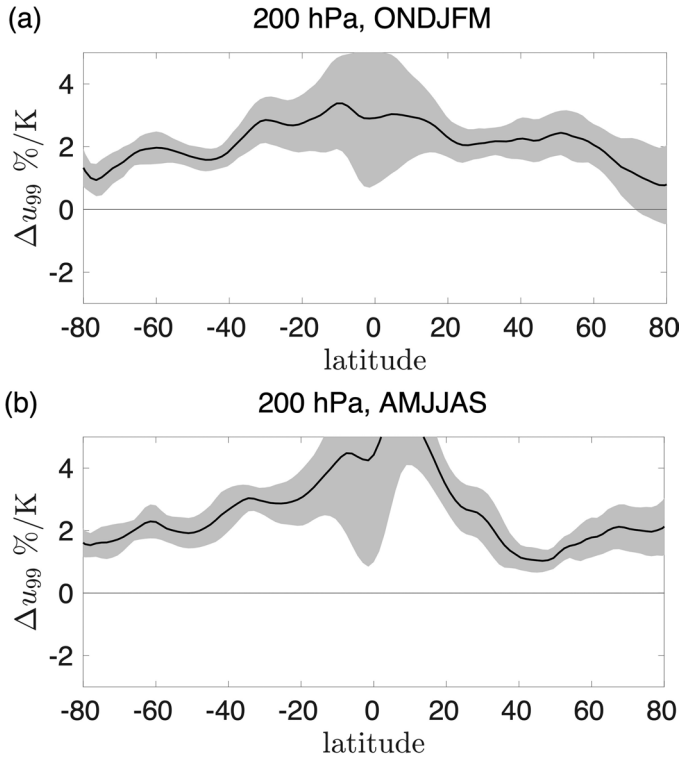

Extended Data Fig. 2 | Fast jet stream winds under climate change across the seasonal cycle. Fractional changes in the fast (> 99th percentile) upper-level (200 hPa) jet stream winds normalized by the global-mean change in surface air temperature for each model for (a) November through March and (b) April through September. Data are presented as multi-model-mean (thick line) ± one standard deviation of the response across the model ensemble (shading).

https://doi.org/10.1038/s41558-023-01884-1

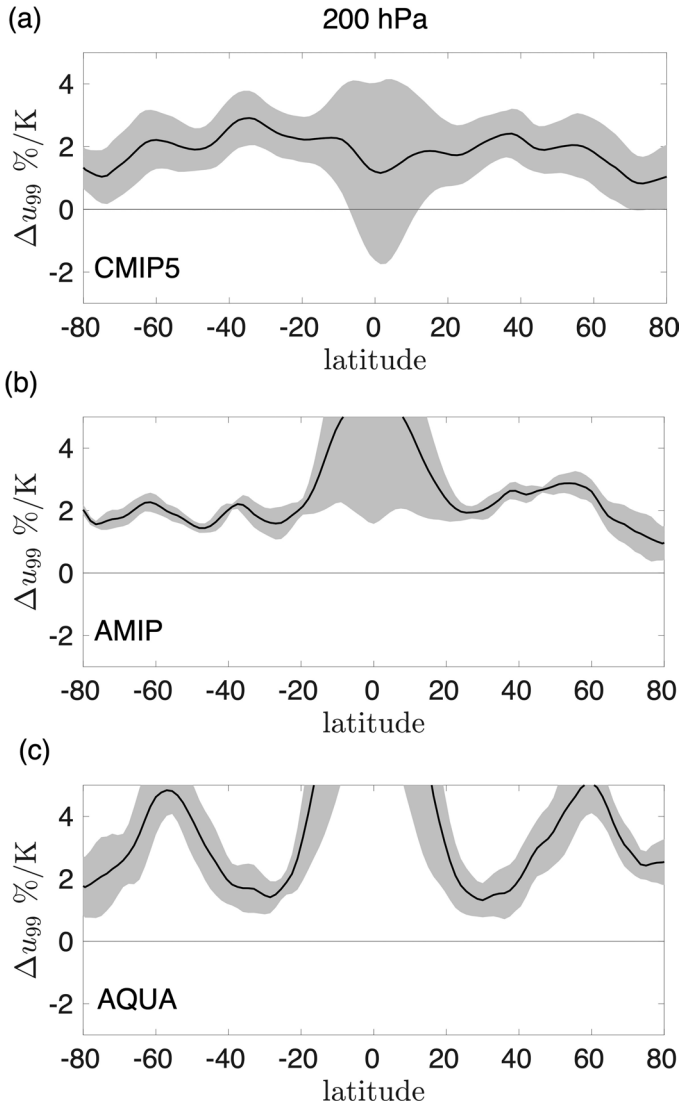

Extended Data Fig. 3 | Fast jet stream winds under climate change across a model hierarchy. Fractional changes in the fast (> 99th percentile) upper-level (200 hPa) jet stream winds normalized by the global-mean change in surface air temperature for each model for (a) CMIP5 RCP8.5 (2080 to 2100) minus historical (1980 to 2000) coupled climate models, (b) CMIP6 amip-p4K minus amip, and (c) CMIP6 aqua-p4K minus aqua. Data are presented as multi-model-mean (thick line) ± one standard deviation of the response across the model ensemble (shading).

https://doi.org/10.1038/s41558-023-01884-1

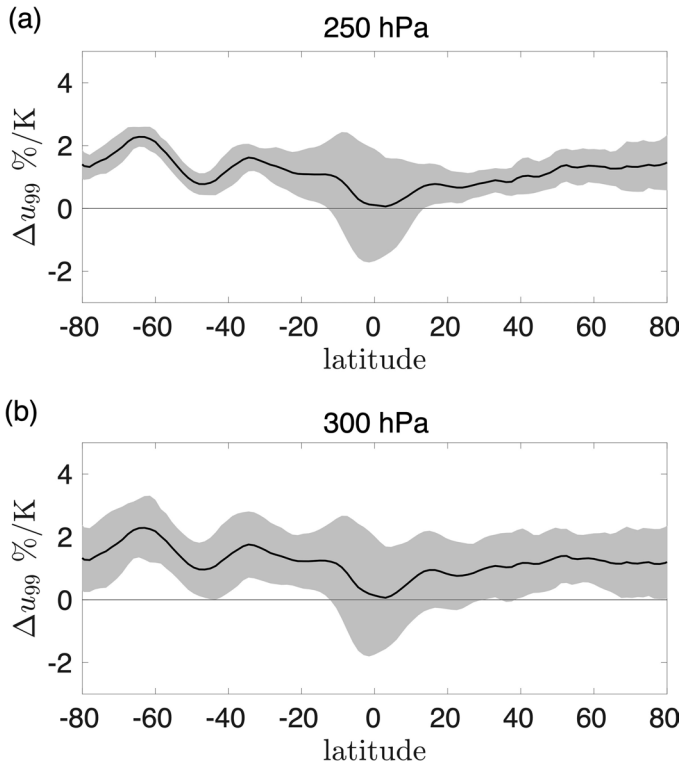

Extended Data Fig. 4 | Fast jet stream winds under climate change across the jet cores. Fractional changes in the fast (> 99th percentile) upper-level (a) 250 hPa and (b) 300 hPa jet stream winds normalized by the global-mean change in surface air temperature for each model for CMIP6 SSP5-8.5 (2080 to 2100) minus historical (1980 to 2000) coupled climate models. Data are presented as multi-model-mean (thick line) ± one standard deviation of the response across the model ensemble (shading).

https://doi.org/10.1038/s41558-023-01884-1

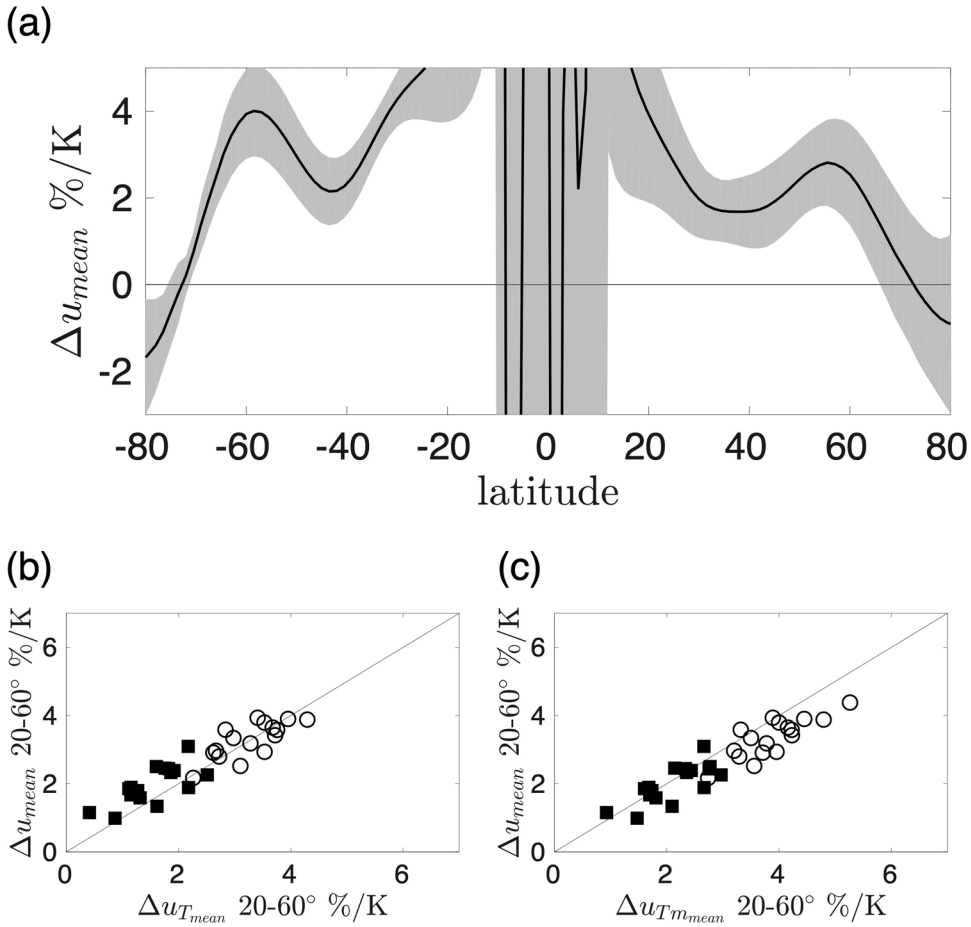

Extended Data Fig. 5 | Average jet stream winds under climate change. (a) Fractional changes in the average daily upper-level (200 hPa) jet stream winds normalized by the global-mean change in surface air temperature for each model. Data are presented as multi-model-mean (thick line) ± one standard deviation of the response across the model ensemble (shading). Fractional changes in the average daily upper-level zonal winds normalized by the global-mean change in surface air temperature for each model versus (b) thermal wind (equation (1)) and (c) moist thermal wind (equation (2)) averaged over the extratropics (20-60° latitude). Northern Hemisphere values from individual models are shown by squares and Southern Hemisphere values are shown by circles.

https://doi.org/10.1038/s41558-023-01884-1

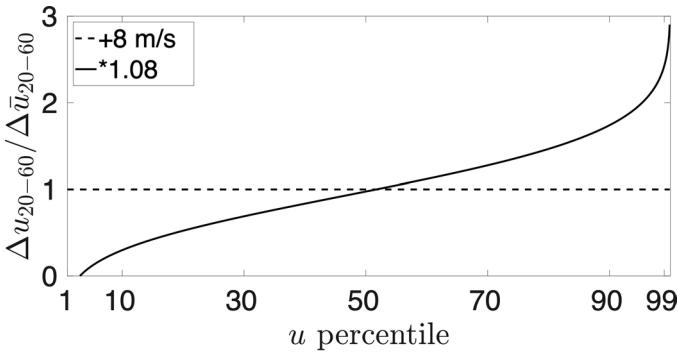

Extended Data Fig. 6 | Jet stream wind distribution response to idealized climate change. Response of distribution of 200 hPa extratropical (20–60 degrees) jet stream winds from 1980 to 2000 in ERA5 to idealized climate change involving a uniform increase of 8 ms^{-1} (additive increase, dashed black) and a 8% increase (multiplicative increase, solid black).

https://doi.org/10.1038/s41558-023-01884-1

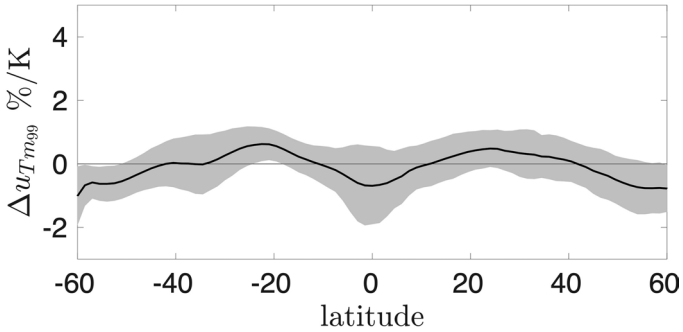

Extended Data Fig. 7 | Residual of moist thermal wind decomposition for fast jet stream wind. Fractional changes in the fast (> 99th percentile) upper-level (200 hPa) moist thermal wind decomposed into contributions from the residual (black) normalized by the global-mean change in surface air temperature for each model (see equation (3)). Data are presented as multi-model-mean (thick line) ± one standard deviation of the response across the model ensemble (shading).

https://doi.org/10.1038/s41558-023-01884-1

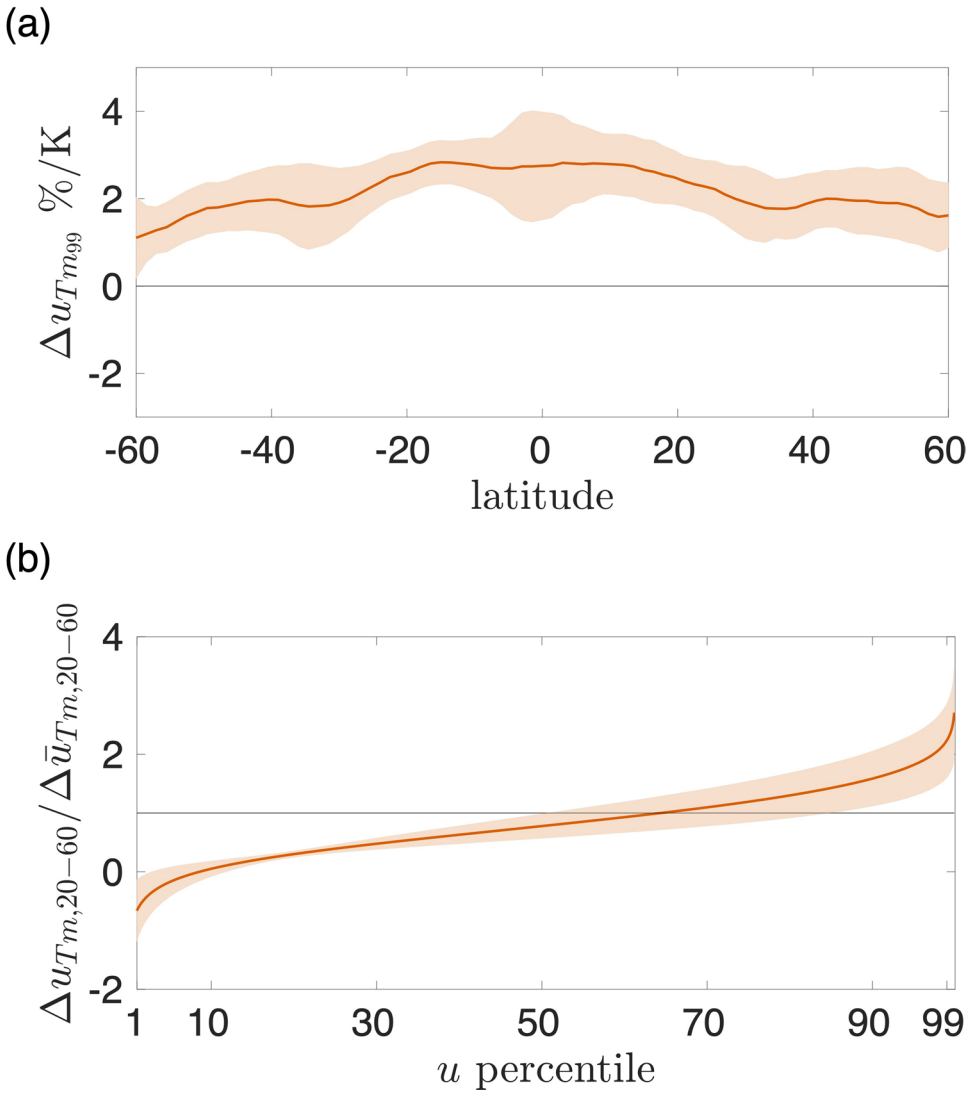

Extended Data Fig. 8 | Relationship between fast jet stream winds and moisture under climate change. (a) Fractional changes in the fast (> 99th percentile) upper-level (200 hPa) moist thermal wind due to the contributions from moist-get-moister response with no change in meridional temperature gradient (meridional saturation entropy gradient following Clausius–Clapeyron) normalized by the global-mean change in surface air temperature for each model. (b) Response of moist thermal wind over the extratropics (20–60° latitude) in both hemispheres across percentiles relative to the response of the average wind ($\bar{u}_{Tm}$) due to the same contributions as (a). Data are presented as multi-model-mean (thick line) ± one standard deviation of the response across the model ensemble (shading).

https://doi.org/10.1038/s41558-023-01884-1

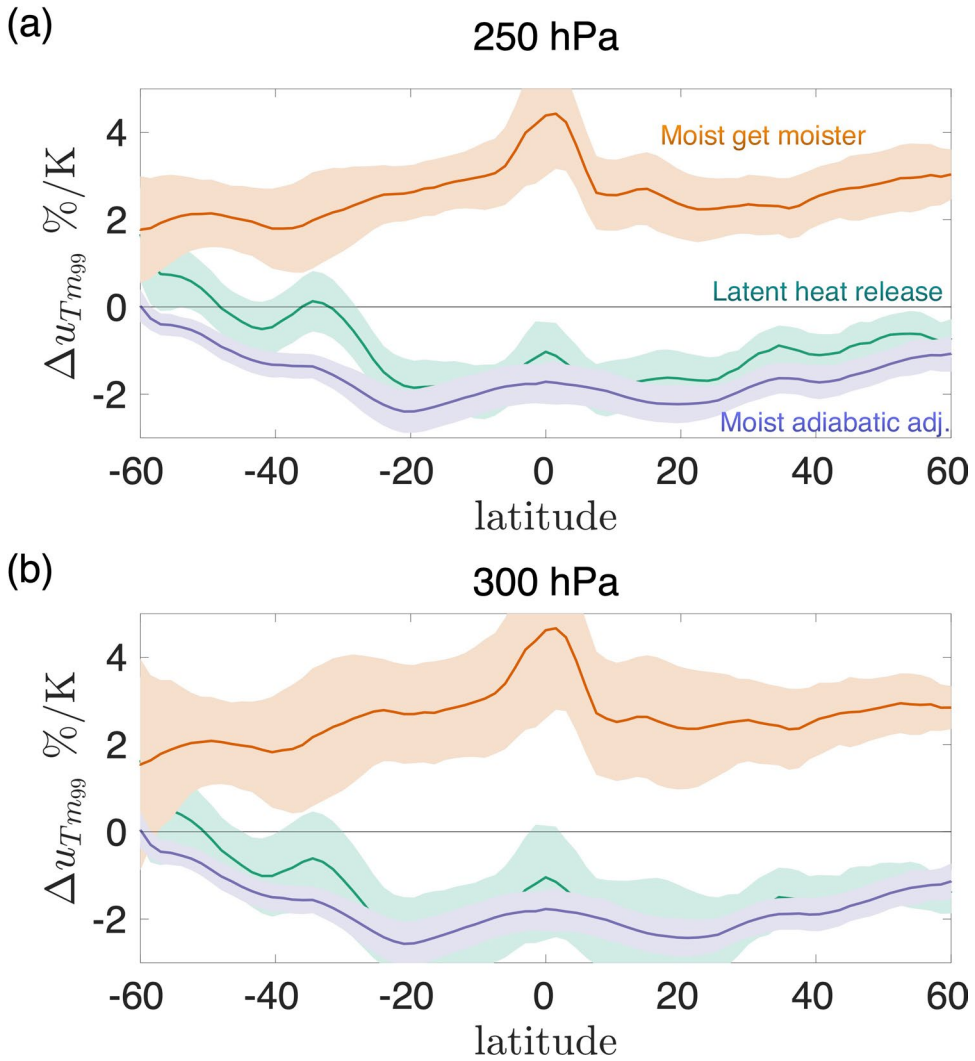

Extended Data Fig. 9 | Relationship between fast jet stream winds and moisture under climate change. Fractional changes in the fast (> 99th percentile) upper-level (200 hPa) moist thermal wind due to the contributions from moist-get-moister, latent heat release and moist adiabatic adjustment responses (see equation (5)) normalized by the global-mean change in surface air temperature for each model at (a) 250 hPa and (b) 300 hPa. Data are presented as multi-model-mean (thick line) ± one standard deviation of the response across the model ensemble (shading).

https://doi.org/10.1038/s41558-023-01884-1

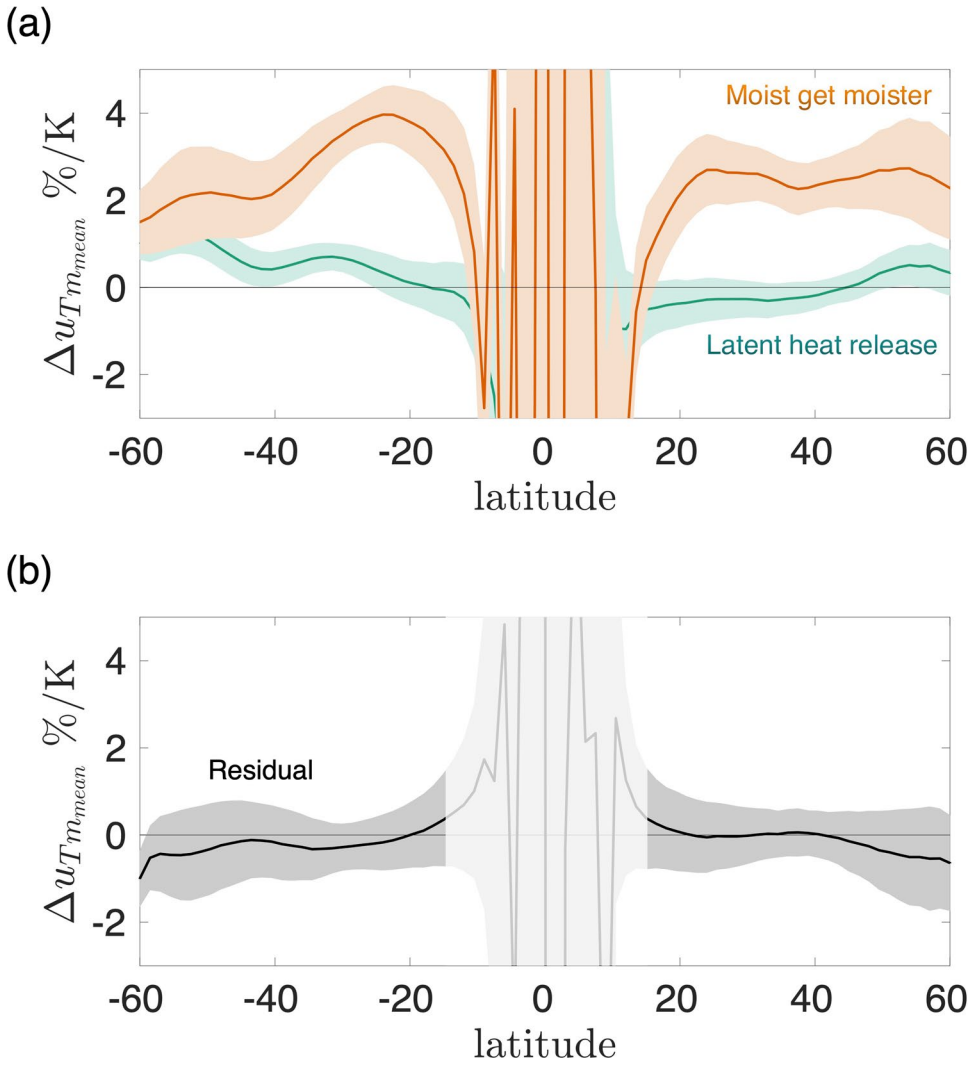

Extended Data Fig. 10 | Relationship between the average jet stream winds and moisture under climate change. (a) Fractional changes in the average4 upper-level (200 hPa) moist thermal wind due to the contributions from changes in latent heat release, moist-get-moister response and moist adiabat normalized by the global-mean change in surface air temperature for each model. (b) Residual of moist thermal wind decomposition of the average jet stream wind response under climate change. Data are presented as multi-model-mean (thick line) ± one standard deviation of the response across the model ensemble (shading).